Thermo-mechanical modeling of dendrite deformation in continuous casting of steel



2012 IOP Conf. Ser.: Mater. Sci. Eng. 33 012058

(http://iopscience.iop.org/1757-899X/33/1/012058)

# Thermo-mechanical modeling of dendrite deformation in continuous casting of steel

**J Domitner[1], J-M Drezet[2], M Wu[3,4] and A Ludwig[1,4]**

[1] Christian Doppler Laboratory for Multiphase Modeling of Metallurgical Processes, University of Leoben, Franz-Josef-Straße 18, 8700 Leoben, Austria
[2] Computational Materials Laboratory, Ecole Polytechnique Fédérale de Lausanne, LSMX MX-G Ecublens, Station 12, 1015 Lausanne, Switzerland
[3] Christian Doppler Laboratory for Advanced Process Simulation of Solidification and Melting, University of Leoben, Franz-Josef-Straße 18, 8700 Leoben, Austria
[4] Chair of Simulation and Modeling of Metallurgical Processes, University of Leoben, Franz-Josef-Straße 18, 8700 Leoben, Austria

E-mail: josef.domitner@unileoben.ac.at

**Abstract**. In the field of modern steelmaking, continuous casting has become the major manufacturing process to handle a wide range of steel grades. An important criterion characterizing the quality of semi-finished cast products is the macrosegregation forming at the centre of these products during solidification. The deformation induced interdendritic melt flow has been identified as the key mechanism for the formation of centreline segregation. Bulging of the solidified strand shell causes deformation of the solidifying dendrites at the casting's centre. Hence, a fundamental knowledge about the solid phase motion during casting processes is crucial to examine segregation phenomena in detail. To investigate dendritic deformation particularly at the strand centre, a thermo-mechanical Finite Element (FE) simulation model is built in the commercial software package ABAQUS. The complex dendritic shape is approximated with a conical model geometry. Varying this geometry allows considering the influence of different centreline solid fractions on the dendrite deformation. A sinusoidal load profile is used to describe bulging of the solid which deforms the dendrites. Based on the strain rates obtained in the FE simulations the dendrite deformation velocity perpendicular to the casting direction is calculated. The velocity presented for different conditions is used as input parameter for computational fluid dynamics (CFD) simulations to investigate macrosegregation formation inside of a continuous casting strand using the commercial software package FLUENT.

## 1. Introduction

Nowadays, continuous strand casting is the main production process to manufacture a wide range of semi-finished steel products. To remain competitive, steelmaking companies must provide their continuous cast products (slabs, billets, blooms) at a desired quality on time, always keeping an eye on the actual production costs. This has become a critical factor of economic success during the past years and it will play an increasingly important role in the future. Hence, a detailed knowledge of the casting process is essential to guarantee stable operating conditions and to gain reproducible product specifications [1].

In particular the formation of macrosegregation [2-3] inside the cast products should be prevented as far as possible, since macrosegregation causes problems in further processing steps. Technical measures like mechanical softreduction (MSR) can reduce but not completely prevent this undesirable defect during casting [4-7]. Since solidification advances from the surface towards the centre, the segregated steel melt (enriched with alloying elements such as carbon, silicon, manganese, etc.) accumulates and finally solidifies at the strand centre. The accumulation is enhanced, if the shrinkage induced flow of unsegregated melt along the casting direction and therefore its mixing with the highly enriched melt is inhibited.

In slab casting, strand shell deformation (e.g. caused by bulging between adjacent guiding rolls of the casting machine) was identified as key mechanism to form positive centreline macrosegregation [8-11]. Strand surface bulging causes a periodic movement of the dendritic mushy zone inside the strand. The motion of the dendrites perpendicular to the casting direction is directly related to the deformation of the solid strand shell. However, if the dendrite trunks meet at the centre of the cast strand at the final stage of solidification, they will deform under compression.

Segregation formation is strongly influenced by relative motion between the growing dendrites and the interdendritic melt [12-14]. Hence, describing the deformation velocity of the dendrites at the strand centreline is essential to simulate macrosegregation formation. Miyazawa et al. proposed that the solid velocity component perpendicular to the casting direction decreases linearly towards the centre [8]. However, Mayer et al. and Domitner et al. used an exponentially decreasing velocity approach to consider that most deformation might occur at the dendritic tip region [11, 15]. To obtain deeper understanding about the actual deformation velocities, a thermo-mechanical Finite Element simulation model was implemented in the commercial software package ABAQUS.

## 2. Thermo-mechanical simulation model

### 2.1. Model geometry

Solidification inside of steel continuous casting strands leads to different complex-shaped dendritic morphologies. Generally, four characteristic morphology types can be distinguished: strictly oriented, mostly oriented, equiaxed and globulitic [9]. While globulitic and equiaxed dendritic solidification occurs mainly at the strand surface, oriented columnar solidification can be observed in regions between the surface and the strand centreline. Occasionally, down-sinking equiaxed crystals can be observed in the central region.

Since the current simulations are focused on investigating the deformation behaviour of columnar dendrites perpendicular to the casting direction, equiaxed crystals are not considered in the model. Besides, the complex columnar dendritic shape is approximated with a conical axisymmetric model geometry, as shown in figure 1. This simplified geometry represents a primary dendrite trunk growing perpendicular to the casting direction $x$ and therefore parallel to the deformation direction $y$. The influence of secondary dendrite arms on the deformation behaviour is neglected. The model geometry has an entire length of $l$ = 30 mm and an overall diameter of $d$ = 1.2 mm. While $d$ is based on a typical primary dendrite arm spacing observed at the centre region of a continuous casting strand [16-17], $l$ is related to the local mushy zone width being estimated by numerical simulation of a 25.0 m long continuous casting strand [15].

The volume fraction of solid varies from the tip to the root of the primary dendrite. As shown in figure 1, the so-called "zero-strength" solid fraction, $f_S^{zero}$, corresponds to the upper boundary of the model geometry, whereas the centreline solid fraction, $f_S^{cent}$, corresponds to the bottom boundary representing the dendrite tip. The tip is assumed to be located at the centreline of the casting strand. In the performed simulations, dendritic deformation occurs only if $f_S < f_S^{zero}$, while the dendrite trunks are assumed to behave rigid if $f_S \geq f_S^{zero}$. The centreline solid fraction, $f_S^{cent}$, is calculated with

$$f_S^{cent} = f_S^{zero}\left(\frac{r^{cent}}{r^{zero}}\right)^2 . \quad (1)$$

In equation (1), $r^{zero}$ stands for the radius of the modeled dendrite at $f_S^{zero}$. It is defined as

$$r^{zero} = \frac{d}{2} = \frac{l}{50}. \tag{2}$$

$r^{cent}$ represents the dendrite's tip radius at the centre of the casting strand. In the performed simulations, five model geometries with $r^{cent}$ = 0.1 mm, 0.2 mm, 0.3 mm, 0.4 mm and 0.5 mm are compared to investigate the influence of different $f_S^{cent}$ on the deformation behaviour. These geometries are depicted in figure 2. The height of the conical region, $h$, depends on $r^{cent}$:

$$h = 50\left(r^{zero} - r^{cent}\right) \tag{3}$$

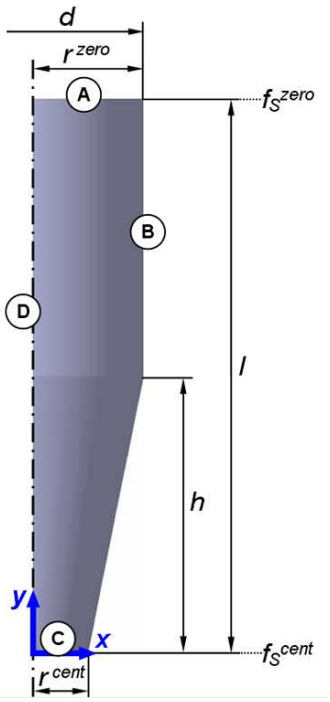


**Figure 1.** 2D axisymmetric model geometry used in the ABAQUS simulations. For visualization, a scaling of $x : y$ = 10:1 is applied. The letters A, B, C and D indicate the position of different boundary conditions.

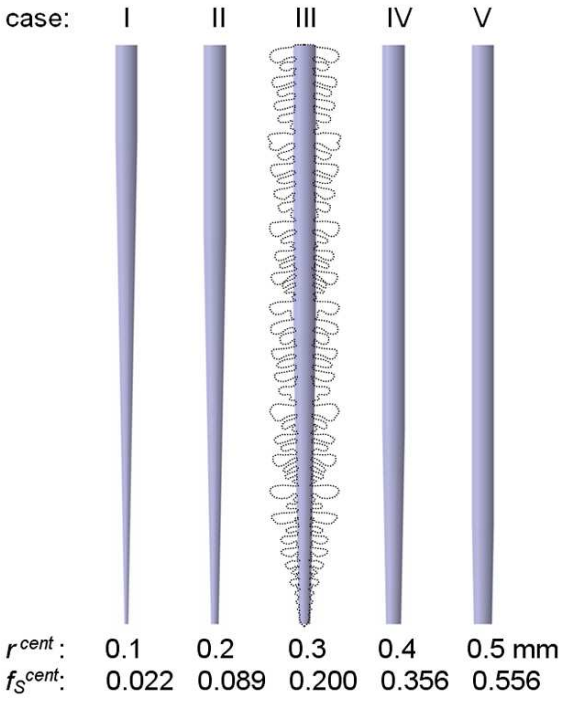


**Figure 2.** Different model geometries used in simulation cases I-V (actual geometry without scaling). For comparison, a dendritic contour including secondary arms is shown schematically at case III.

2.2. Boundary conditions

In figure 1, four boundaries ("A", "B", "C" and "D") are marked. At the upper boundary "A" a sinusoidal displacement is applied to deform the dendrite in $y$-direction. This load represents a single bulging cycle between two adjacent guiding rolls at a continuous casting plant. Figure 3 shows the time-dependent load profiles, displacement and corresponding solid velocity, $v_{S,y}^{zero}$. It is assumed that the maximum bulging amplitude decreases linearly from 0.8 mm at the exit of the continuous casting mould (strand coordinate $X$ = 0.0 m, corresponding casting time $T$ = 0.0 s) to 0.0 mm at the zone of strand end solidification (strand coordinate $X$ = 22.5 m, corresponding casting time $T$ = 1800.0 s). Hence, the bulging profile shown in figure 3 is obtained for $X$ = 16.5 m where solidification and therefore the growing dendrites reach the strand centreline. Details about the bulging profile definition are given in [15].

Furthermore, no horizontal deformation in $x$-direction is allowed at the right boundary "B", whereas vertical movement in $y$-direction is hindered at the bottom boundary "C". To simulate a 2D axisymmetric problem, boundary "D" is treated as rotational symmetry axis.

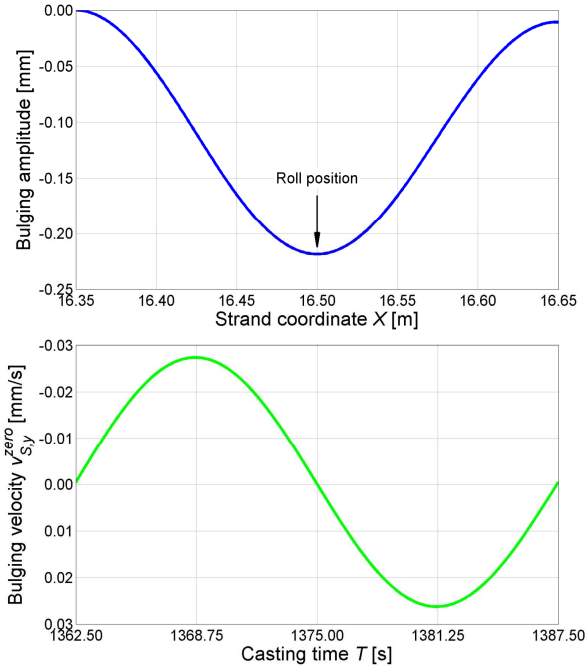


**Figure 3.** Load profiles used in all of the five simulation cases to deform the dendrites.

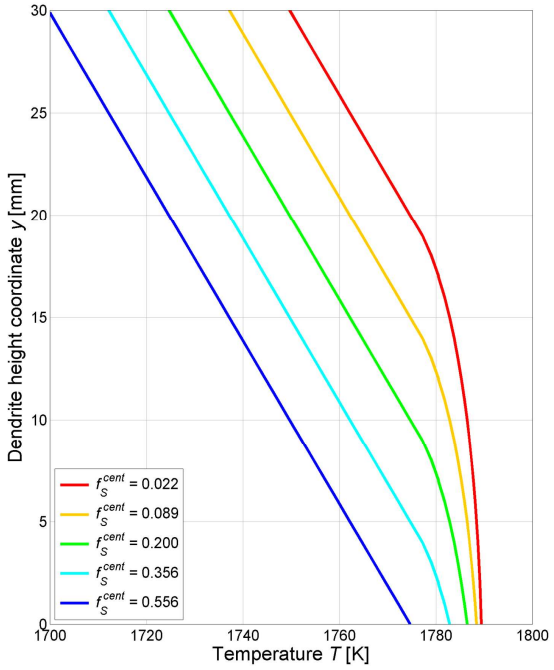


**Figure 4.** Solid fraction dependent temperature profiles for simulation cases I-V.

## 2.3. Numerical model

### *2.3.1. Thermal conditions*

Since the mechanical properties are temperature dependent, the temperature varying only in $y$-direction within the dendrite is imposed in the ABAQUS simulations. Two temperature regimes are distinguished in the model. For $f_S < 0.5$ the temperature is calculated according to Scheil for a binary Fe-C-alloy, as given in equation (4). For $f_S > 0.5$ a linearly decreasing temperature is imposed using equation (5), where $G$ is the uniform temperature gradient at the dendrite axis. Equations (4) and (5) approximate the temperature profiles which were obtained by modeling solidification inside a 25.0 m long continuous casting strand [15]. The data required to calculate the axial temperature profiles are given in table 1; the resulting temperature profiles used for simulation cases I-V are shown in figure 4.

$$T\left(f_S < 0.5\right) = T_m + C_{L,0}^{C}\, m \left(1 - f_S\right)^{k-1} \tag{4}$$

$$T\left(f_S > 0.5\right) = T\left(f_S = 0.5\right) - G\left(y - y\left(f_S = 0.5\right)\right) \tag{5}$$

**Table 1.** Data to calculate the temperature profiles

| | |
|---|---|
| Melting temperature $T_m$ | 1790 K |
| Initial carbon concentration $C_{L,0}^{C}$ | 0.182 wt.% |
| Liquidus slope $m$ | -116.7 K/wt.% |
| Distribution coefficient $k$ | 0.36 |
| Temperature gradient $G$ | 2500 K/m |

*2.3.2. Mechanical properties*

Two contributions are considered in the mechanical model for calculating the strain rate tensor $\dot{\boldsymbol{\varepsilon}}$, namely the elastic strain rate $\dot{\boldsymbol{\varepsilon}}_{el}$ and the viscoplastic strain rate $\dot{\boldsymbol{\varepsilon}}_{vp}$:

$$\dot{\boldsymbol{\varepsilon}} = \dot{\boldsymbol{\varepsilon}}_{el} + \dot{\boldsymbol{\varepsilon}}_{vp} \tag{6}$$

According to Hooke's law, $\dot{\boldsymbol{\varepsilon}}_{el}$ depends on the stress tensor $\boldsymbol{\sigma}$ and on the elasticity tensor $\mathbf{D}_{el}$, which is defined by the Young's modulus $E(T)$ and the Poisson's ratio $\mu$:

$$\dot{\boldsymbol{\varepsilon}}_{el} = \mathbf{D}_{el}^{-1}\,\dot{\boldsymbol{\sigma}} \tag{7}$$

Considering only creep deformation at high temperatures, $\dot{\boldsymbol{\varepsilon}}_{vp}$ is expressed as

$$\dot{\boldsymbol{\varepsilon}}_{vp} = \frac{3\dot{\varepsilon}_{vp}^{eq}}{2\sigma^{eq}}\mathbf{s}, \tag{8}$$

where $\mathbf{s}$ stands for the deviatoric tensor and $\sigma^{eq}$ is the Von Mises equivalent stress. $\dot{\varepsilon}_{vp}^{eq}$ represents the equivalent viscoplastic strain rate, which is defined as:

$$\dot{\varepsilon}_{vp}^{eq} = A\,\mathrm{e}^{-\frac{Q}{\mathrm{R}T}}\left(\sinh\left(a_\sigma\sigma^{eq}\right)\right)^n \tag{9}$$

In equation (9), R is the universal gas constant and $Q$ is the activation energy. Further details about defining the parameters $Q$, $A$, $a_\sigma(T)$, $n(T)$, $E(T)$ and $\mu$ can be found in [10].

## 3. Results and discussion

3.1. Thermo-mechanical simulations

The local deformation velocity in $y$-direction within a given mesh element $i$, $v_{S,y}(i)$, is calculated with equation (10). Therein, $\dot{\varepsilon}_y(i)$ represents the $y$-component of the strain rate tensor obtained by the ABAQUS simulations. $\Delta y(i)$ stands for the height of the element located at the dendrite axis ($x$ = 0 mm).

$$v_{S,y}(i) = \dot{\varepsilon}_y(i)\,\Delta y(i) \tag{10}$$

Furthermore, equation (11) is used to determine $v_{S,y}(n)$, the total deformation velocity of the mesh element $n$. Starting at element $i$ = 1 located at the dendrite tip, the velocities $v_{S,y}(i)$ are summed up for $i = 1 \ldots n$.

$$v_{S,y}(n) = \sum_{i=1}^{n} v_{S,y}(i) \tag{11}$$

The total number of mesh elements along the dendrite axis, $N$, is constant for each of the five simulation cases ($N$ = 60). According to the applied boundary conditions, $v_{S,y}(0) = 0$ at $y$ = 0 mm and $v_{S,y}(N) = v_{S,y}^{zero}$ at $y$ = 30 mm.

As an example, figure 5 shows the velocity profiles obtained for simulation case III at different times using equation (11). These results are focused on the first half of the bulging cycle when the casting strand is compressed in front of a guiding roll. It is assumed that only this compression causes the deformation of the dendrites at the strand centre. Due to the negligible elastic contribution at high temperature no deformation (expansion) occurs when the strand widens behind the roll. Since dendrite deformation acts against the positive $y$-direction, the obtained values of $v_{S,y}$ have a negative sign.

The bulging cycle retained for the simulation starts at the casting time $T$ = 1362.5 s, which corresponds to the bulging cycle time $t$ = 0.00 s. At this moment $v_{S,y}^{zero}$ = 0 and therefore $v_{S,y}$ = 0 too. Hence, the velocity profile is a straight horizontal line for $t$ = 0.00 s, as depicted in figure 5 (a). However, with advancing bulging time $v_{S,y}$ increases in amplitude until maximum values are reached

at $t = 6.25$ s. This results in a strongly curved velocity profile. Then, the velocity $v_{S,y}$ decreases until $v_{S,y} = 0$ at $t = 12.50$ s, which is shown again with a horizontal line in figure 5 (a). For each of the velocity profiles displayed in figure 5, $v_{S,y} = 0$ at the centerline solid fraction $f_S^{cent} = 0.20$.

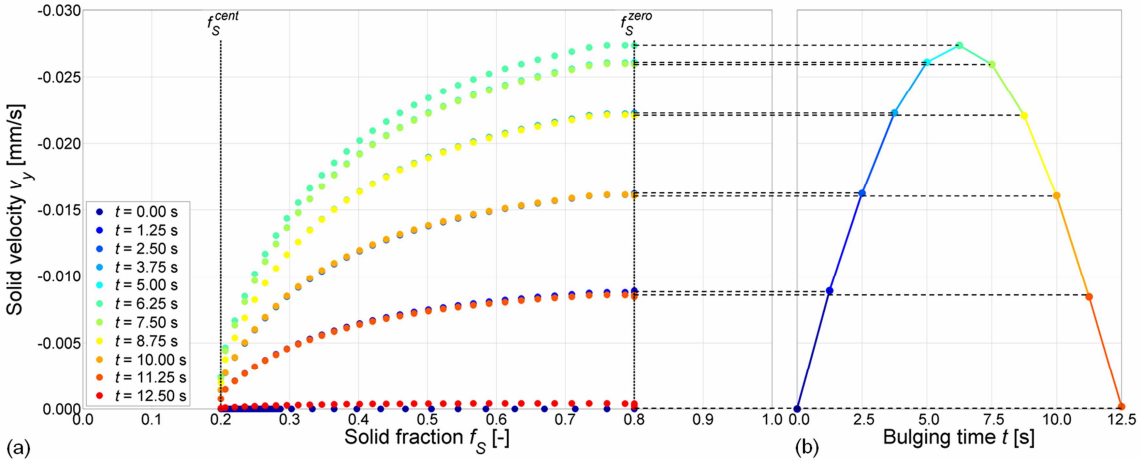


**Figure 5.** Profiles of solid velocity $v_{S,y}$ between $f_S^{cent}$ and $f_S^{zero}$ (a) and evolution of the corresponding maximum velocity at $f_S^{zero}$ (b). The profiles are calculated for simulation case III.

Figure 6 compares the velocity profiles at $t = 6.25$ s calculated for simulation cases I-V. For each of these profiles, $v_{S,y} = 0$ at the centerline solid fraction $f_S^{cent}$ and $v_{S,y} = v_{S,y}^{zero}$ at the zero-strength solid fraction $f_S^{zero}$. Since the bulging velocity profile shown in figure 3 is used for simulation cases I-V, $v_{S,y}^{zero}$ is identical for each case at a particular time $t$. Equations (12) and (13) are suggested to fit the calculated velocities for solid fractions between $f_S^{cent}$ and $f_S^{zero}$:

$$v_{S,y} = v_{S,y}^{zero}\left(1 - f_S^{\Psi}\right) \tag{12}$$

$$\Psi = a\frac{\left(f_S^{cent} - f_S\right)}{\left(f_S^{zero} - f_S\right)^b} \tag{13}$$

In equation (13), $a$ and $b$ are dimensionless fit constants. With $a = 4.0$ and $b = 0.8$ the fitting curves approximate relatively well the obtained simulation data. Exemplary, the fitted velocity profiles at the maximum bulging amplitude (bulging time $t = 6.25$ s) are shown in figure 6.

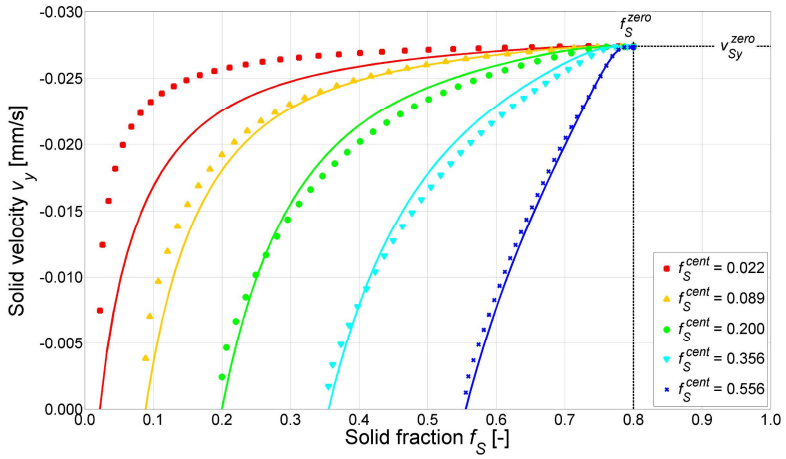


**Figure 6.** Velocity profiles at $t = 6.25$ s for simulation cases I-V. Each dot marks the calculated velocity $v_{S,y}$ at a certain mesh element. The continuous lines are fitting curves of $v_{S,y}$.

As shown in figure 6, equations (12) and (13) are suitable to fit the results of simulation cases II-V, but they do not fit the results of case I. Thus, these comparatively simple fit equations are not applicable to very small solid fractions. Nevertheless, this can be accepted, since previous simulations have shown that small solid fractions at the strand centre have only a minor influence on the formation of centreline macrosegregation [15].

### 3.2. Solidification simulations

The obtained relationship between solid fraction and deformation velocity is then used for fluid flow simulations to predict macrosegregation formation in steel continuous casting. For this reason, a two dimensional horizontal continuous casting strand is modeled. Details about the 25 m long strand geometry and about the basic model definitions are explained in [15], where the exponential approach of equation (14) is used instead of equation (12) to describe the dendrite deformation. However, the function $\Psi$ in equation (14) is calculated with equation (13), but with $a = 50$ and $b = 0.25$.

$$v_{S,y} = v_{S,y}^{zero}\left(1 - \mathrm{e}^{\Psi}\right) \tag{14}$$

The fundamental conservation equations used for the numerical multiphase model in [15] as well as in the current paper are described in [18-21]. Although this model basically includes three phases, the equiaxed phase is not considered in the current simulations. According to equation (15) the mixture concentration of carbon, $C_M^{\mathrm{C}}$, is defined to quantify the macrosegregation. In this equation, $\rho_S$ and $\rho_L$ are the densities of the solid and of the liquid phase. $C_S^{\mathrm{C}}$ and $C_L^{\mathrm{C}}$ represent the carbon concentrations within solid and liquid, $f_S$ and $f_L$ are the volume fractions of both phases.

$$C_M^{\mathrm{C}} = \frac{\rho_S \cdot C_S^{\mathrm{C}} \cdot f_S + \rho_L \cdot C_L^{\mathrm{C}} \cdot f_L}{\rho_S \cdot f_S + \rho_L \cdot f_L} \tag{15}$$

Figure 7 (b) shows the macrosegregation profiles of carbon obtained at the outlet of the simulation domain considering solid phase velocities after equations (12) (present work) and (14) (exponential approach [15]), respectively. At the outlet position, the cross-section of the continuous casting strand is totally solid ( $f_S > 0.95$). Hence, it is not possible to modify the macrosegregation being observed at this position. The simulations deliver the typical macrosegregation profiles occurring in continuous casting of steel: a strongly positive segregation peak at the strand centre accompanied with a negative segregation valley beside.

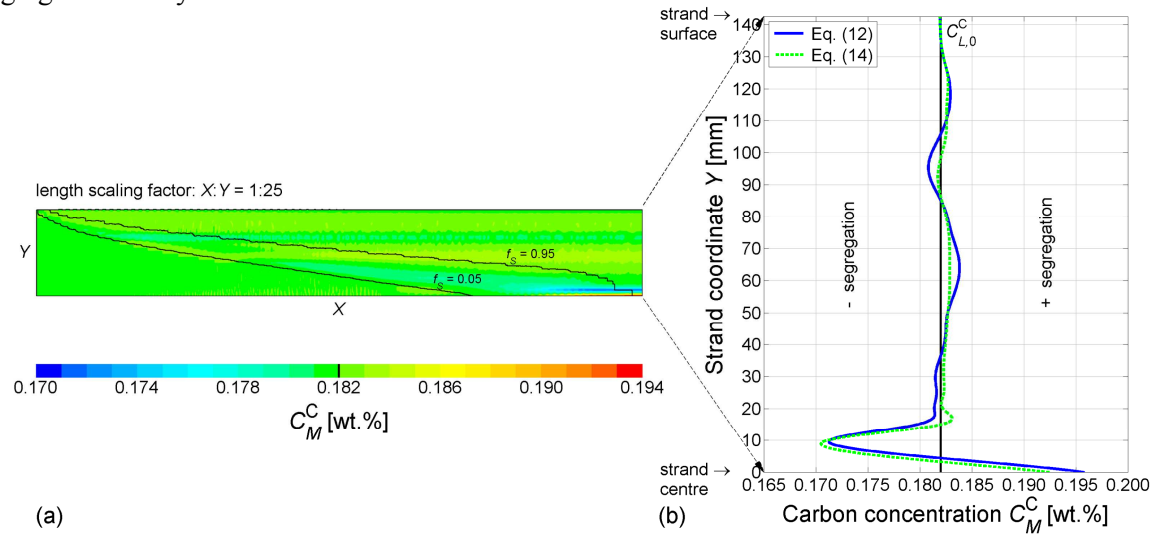


**Figure 7.** Typical macrosegregation pattern (a) and smoothed segregation profiles at the outlet of the modeled casting strand (b). Continuous blue line: velocity definition after equation (12), dashed green line: velocity definition after equation (14), black line: initial concentration of carbon.

## 4. Conclusions

In the current paper, a general possibility to combine thermo-mechanical simulations of deforming dendrites at microscale level with CFD simulations to predict centreline segregation formation in continuous casting at macroscale level is presented. In the numerical two-phase model used for CFD simulations, the solid phase velocities in both coordinate directions must be predefined. Particularly, quantifying the deformation speed of the solid dendrites at the strand centre is necessary, which is achieved with thermo-mechanical simulations. Therein, the complex dendritic morphology is approximated with a simple conical model geometry being compressed with a sinusoidal load amplitude representing strand bulging during the casting process.

The simulation results indicate that the dendritic deformation velocity is immediately influenced by the solid fraction at the centreline of the casting strand. For low centreline solid fractions, dendritic deformation is concentrated at the dendrite tips at the strand centre region. In this case a comparatively rapid decay of the solid velocity at the centre can be observed. However, with increasing centreline solid fractions the deformation zone extends along the dendrite axis. Based on these simulation results a relationship is proposed to describe the deformation velocity depending on the solid fraction. This relationship is then used in subsequent CFD-simulations to examine macrosegregation formation in strand casting. The results show a strongly positive segregation peak at the strand centre accompanied with a negative segregation valley beside, which is typical for strand casting of steel.

Due to a lack of geometry data, the complex dendritic morphology is simplified in the current thermo-mechanical simulations. Thus, the influence of side arms and the interaction of adjacent dendrites particularly at higher solid fractions are not considered. Simulations using more realistic dendritic morphologies captured with experimental methods (e.g. X-ray computed tomography or X-ray synchrotron analysis, serial sectioning techniques, etc.) would be of further interest to improve the understanding of the deformation behaviour.

## References

[1] Brimacombe J K 1999 *Metall. Mater. Trans.* B **30B** 553-66
[2] Flemings M C 2000 *ISIJ Int.* **40** 833-41
[3] Lesoult G 2005 *Mater. Sci. Eng.* A **413-414** 19-29
[4] Reichert A, Tacke K-H, Harste K, Hecht M, Heilemann J, Ölmann U, Schwerdtfeger K, Barber B, Beaverstock C and Walmsley R 2002 *Casting and solidification - Strand reduction in continuous casting and its effect on product quality* (Luxembourg: European Communities)
[5] Thome R and Harste K 2004 *Steel Res. Int.* **75** 693-700
[6] Bleck W, Wang W and Bülte R 2006 *Steel Res. Int.* **77** 485-91
[7] Thome R and Harste K 2006 *ISIJ Int.* **46** 1839-44
[8] Miyazawa K and Schwerdtfeger K 1981 *Arch. Eisenhüttenwesen* **52** 415-22
[9] Stadler P, Hagen K, Hammerschmid P and Schwerdtfeger K 1982 *Stahl Eisen* **102** 451-59
[10] Kajitani T, Drezet J-M and Rappaz M 2001 *Metall. Mater. Trans.* A **32A** 1479-91
[11] Mayer F, Wu M and Ludwig A 2011 *Steel Res. Int.* **81** 660-67
[12] Beckermann C 2002 *Int. Mater. Rev.* **47** 243-61
[13] Schwerdtfeger K and Heilemann J 2006 *ISIJ Int.* **46** 70-74
[14] Eisermann H and Schwerdtfeger K 2006 *ISIJ Int.* **46** 75-81
[15] Domitner J, Wu M, Mayer F, Ludwig A, Kaufmann B, Reiter J and Schaden T 2011 *Simulations and modelling of solidification and continuous casting processes: Proc. Europ. Conf. on Continuous Casting (Düsseldorf)* S6.1-6
[16] El-Bealy M and Thomas B G 1996 *Metall. Mater. Trans.* B **27B** 689-93
[17] Cicutti C, Bilmes P and Boeri R 1997 *Acta Metall.* **37** 599-604
[18] Ludwig A and Wu M 2005 *Mater. Sci. Eng.* A **413-414** 109-14
[19] Wu M and Ludwig A 2006 *Metall. Mater. Trans.* A **37A** 1613-31
[20] Wu M and Ludwig A 2007 *Metall. Mater. Trans.* A **38A** 1465-75
[21] Wu M, Domitner J and Ludwig A 2012 *Metall. Mater. Trans.* A **43A** 945-64